The Meteoritical Society

Meteoritics & Planetary Science 1–14 (2024)
doi: 10.1111/maps.14279

Zirconium isotope composition indicates *s*-process depletion in samples returned from asteroid Ryugu

Maria SCHÖNBÄCHLER[1]*, Manuela A. FEHR[1], Tetsuya YOKOYAMA[2], Ikshu GAUTAM[2], Nao NAKANISHI[2,3], Yoshinari ABE[4], Jérôme ALÉON[5], Conel ALEXANDER[6], Sachiko AMARI[7,8], Yuri AMELIN[9], Ken-ichi BAJO[10], Martin BIZZARRO[11], Audrey BOUVIER[12], Richard W. CARLSON[6], Marc CHAUSSIDON[13], Byeon-Gak CHOI[14], Nicolas DAUPHAS[15], Andrew M. DAVIS[15], Tommaso DI ROCCO[16], Wataru FUJIYA[17], Ryota FUKAI[18], Makiko K. HABA[2], Yuki HIBIYA[19], Hiroshi HIDAKA[20], Hisashi HOMMA[21], Peter HOPPE[22], Gary R. HUSS[23], Kiyohiro ICHIDA[24], Tsuyoshi IIZUKA[25], Trevor IRELAND[26], Akira ISHIKAWA[2], Shoichi ITOH[27], Noriyuki KAWASAKI[10], Noriko T. KITA[28], Koki KITAJIMA[28], Thorsten KLEINE[29], Shintaro KOMATANI[24], Alexander N. KROT[23], Ming-Chang LIU[30], Yuki MASUDA[2], Mayu MORITA[24], Kazuko MOTOMURA[31], Frédéric MOYNIER[13], Izumi NAKAI[32], Kazuhide NAGASHIMA[23], Ann NGUYEN[33], Larry NITTLER[6], Morihiko ONOSE[24], Andreas PACK[16], Changkun PARK[34], Laurette PIANI[35], Liping QIN[36], Sara RUSSELL[37], Naoya SAKAMOTO[38], Lauren TAFLA[30], Haolan TANG[36], Kentaro TERADA[39], Yasuko TERADA[40], Tomohiro USUI[18], Sohei WADA[10], Meenakshi WADHWA[41], Richard J. WALKER[42], Katsuyuki YAMASHITA[43], Qing-Zhu YIN[44], Shigekazu YONEDA[45], Edward D. YOUNG[30], Hiroharu YUI[46], Ai-Cheng ZHANG[47], Tomoki NAKAMURA[48], Hiroshi NARAOKA[49], Takaaki NOGUCHI[27], Ryuji OKAZAKI[49], Kanako SAKAMOTO[18], Hikaru YABUTA[50], Masanao ABE[18], Akiko MIYAZAKI[18], Aiko NAKATO[18], Masahiro NISHIMURA[18], Tatsuaki OKADA[18], Toru YADA[18], Kasumi YOGATA[18], Satoru NAKAZAWA[18], Takanao SAIKI[18], Satoshi TANAKA[18], Fuyuto TERUI[51], Yuichi TSUDA[18], Sei-ichiro WATANABE[20], Makoto YOSHIKAWA[18], Shogo TACHIBANA[52], and Hisayoshi YURIMOTO[10]

[1]Department of Earth Sciences, Institute for Geochemistry and Petrology, ETH Zurich, Zurich, Switzerland
[2]Department of Earth and Planetary Sciences, Tokyo Institute of Technology, Tokyo, Japan
[3]Department of Earth Sciences, Waseda University, Tokyo, Japan
[4]Graduate School of Engineering, Tokyo Denki University, Tokyo, Japan
[5]Institut de Minéralogie, de Physique des Matériaux et de Cosmochimie, Sorbonne Université, Museum National d'Histoire Naturelle, CNRS UMR 7590, IRD, Paris, France
[6]Earth and Planets Laboratory, Carnegie Institution for Science, Washington, DC, USA
[7]McDonnell Center for the Space Sciences and Physics Department, Washington University, St. Louis, Missouri, USA
[8]Geochemical Research Center, The University of Tokyo, Tokyo, Japan
[9]Korea Basic Science Institute, Ochang, Cheongwon, Cheongju, Chungbuk, Republic of Korea
[10]Department of Natural History Sciences, Hokkaido University, Sapporo, Japan
[11]Centre for Star and Planet Formation, GLOBE Institute, University of Copenhagen, Copenhagen, Denmark
[12]Bayerisches Geoinstitut, Universität Bayreuth, Bayreuth, Germany
[13]Université Paris Cité, Institut de physique du globe de Paris, CNRS, Paris, France
[14]Department of Earth Science Education, Seoul National University, Seoul, Republic of Korea
[15]Department of the Geophysical Sciences and Enrico Fermi Institute, The University of Chicago, Chicago, Illinois, USA
[16]Faculty of Geosciences and Geography, University of Göttingen, Göttingen, Germany
[17]Faculty of Science, Ibaraki University, Mito, Japan
[18]ISAS/JSEC, JAXA, Sagamihara, Japan
[19]Research Center for Advanced Science and Technology, The University of Tokyo, Tokyo, Japan
[20]Department of Earth and Planetary Sciences, Nagoya University, Nagoya, Japan
[21]Osaka Application Laboratory, SBUWDX, Rigaku Corporation, Osaka, Japan
[22]Max Planck Institute for Chemistry, Mainz, Germany

[23]Hawai'i Institute of Geophysics and Planetology, University of Hawai'i at Mānoa, Honolulu, Hawaii, USA
[24]Analytical Technology, Horiba Techno Service Co., Ltd., Kyoto, Japan
[25]Department of Earth and Planetary Science, The University of Tokyo, Tokyo, Japan
[26]School of Earth and Environmental Sciences, The University of Queensland, St Lucia, Queensland, Australia
[27]Division of Earth and Planetary Sciences, Kyoto University, Kyoto, Japan
[28]Department of Geoscience, University of Wisconsin-Madison, Madison, Wisconsin, USA
[29]Max Planck Institute for Solar System Research, Göttingen, Germany
[30]Department of Earth, Planetary, and Space Sciences, UCLA, Los Angeles, California, USA
[31]Thermal Analysis, Rigaku Corporation, Tokyo, Japan
[32]Department of Applied Chemistry, Tokyo University of Science, Tokyo, Japan
[33]Astromaterials Research and Exploration Science, NASA Johnson Space Center, Houston, Texas, USA
[34]Earth-System Sciences, Korea Polar Research Institute, Incheon, Korea
[35]Centre de Recherches Pétrographiques et Géochimiques, CNRS - Université de Lorraine, Nancy, France
[36]CAS Key Laboratory of Crust-Mantle Materials and Environments, University of Science and Technology of China, School of Earth and Space Sciences, Anhui, China
[37]Department of Earth Sciences, Natural History Museum, London, UK
[38]Isotope Imaging Laboratory, Creative Research Institution, Hokkaido University, Sapporo, Japan
[39]Department of Earth and Space Science, Osaka University, Osaka, Japan
[40]Spectroscopy and Imaging, Japan Synchrotron Radiation Research Institute, Hyogo, Japan
[41]School of Earth and Space Exploration, Arizona State University, Tempe, Arizona, USA
[42]Department of Geology, University of Maryland, College Park, Maryland, USA
[43]Graduate School of Natural Science and Technology, Okayama University, Okayama, Japan
[44]Department of Earth and Planetary Sciences, University of California, Davis, California, USA
[45]Department of Science and Engineering, National Museum of Nature and Science, Tsukuba, Japan
[46]Department of Chemistry, Tokyo University of Science, Tokyo, Japan
[47]School of Earth Sciences and Engineering, Nanjing University, Nanjing, China
[48]Department of Earth Science, Tohoku University, Sendai, Japan
[49]Department of Earth and Planetary Sciences, Kyushu University, Fukuoka, Japan
[50]Earth and Planetary Systems Science Program, Hiroshima University, Higashi-Hiroshima, Japan
[51]Kanagawa Institute of Technology, Atsugi, Japan
[52]UTokyo Organization for Planetary and Space Science, The University of Tokyo, Tokyo, Japan

***Correspondence**
Maria Schönbächler, Department of Earth Sciences, Institute for Geochemistry and Petrology, ETH Zurich, 8092 Zurich, Switzerland.
Email: mariasc@ethz.ch

(Received 08 December 2023; revision accepted 12 October 2024)

Abstract–Nucleosynthetic isotope variations are powerful tracers to determine genetic relationships between meteorites and planetary bodies. They can help to link material collected by space missions to known meteorite groups. The Hayabusa 2 mission returned samples from the Cb-type asteroid (162173) Ryugu. The mineralogical, chemical, and isotopic characteristics of these samples show strong similarities to carbonaceous chondrites and in particular CI chondrites. The nucleosynthetic isotope compositions of Ryugu overlap with CI chondrites for several elements (e.g., Cr, Ti, Fe, and Zn). In contrast to these isotopes, which are of predominately supernovae origin, *s*-process variations in Mo isotope data are similar to those of carbonaceous chondrites, but even more *s*-process depleted. To further constrain the origin of this depletion and test whether this signature is also present for other *s*-process elements, we report Zr isotope compositions for three bulk Ryugu samples (A0106, A0106-A0107, C0108) collected from the Hayabusa 2 mission. The data are complemented with that of terrestrial rock reference materials, eucrites, and carbonaceous chondrites. The Ryugu samples are characterized by distinct ^{96}Zr enrichment relative to Earth, indicative of a *s*-process depletion. Such depletion is also observed for carbonaceous chondrites and eucrites, in line with previous Zr isotope work, but it is more extreme in Ryugu, as observed for Mo isotopes. Since *s*-process Zr and Mo are coupled in

mainstream SiC grains, these distinct *s*-process variations might be due to SiC grain depletion in the analyzed materials, potentially caused by incomplete sample digestion, because the Ryugu samples were dissolved on a hotplate only to avoid high blank levels for other elements (e.g., Cr). However, local depletion of SiC grains cannot be excluded. An alternative, equally possible scenario is that aqueous alteration redistributed anomalous, *s*-process-depleted, Zr on a local scale, for example, into Ca-phosphates or phyllosilicates.

INTRODUCTION

The Hayabusa 2 mission returned 5.4 g material from the surface of the Cb-type asteroid (162173) Ryugu. The samples were collected during two touchdown sequences in February and July 2019 (Tachibana et al., 2022). Subsequent analyses of the returned material revealed a striking similarity to CI chondrites based on chemical and isotopic compositions (Nakamura et al., 2022; Yokoyama et al., 2023a). For example, the nucleosynthetic Cr, Ti, Fe, and Zn isotope data from Ryugu samples overlap with those of CI chondrites (Hopp et al., 2022; Paquet et al., 2023; Yokoyama et al., 2023a, 2023b). This indicates that the Ryugu material formed outside the snowline in the protoplanetary disk and originates from the outer solar system. There are also exceptions. Magnesium isotope data hint towards possible nucleosynthetic heterogeneities between Ryugu and CI chondrites (Bizzarro et al., 2023). While the Ti, Fe, and Zn isotope data are largely uniform within Ryugu samples, the $^{54}Cr/^{52}Cr$ ratio varies between different sample aliquots of <25 mg in size (Yokoyama et al., 2023b). Nevertheless, the average Cr isotope composition corresponding to ~90 mg of the bulk Ryugu sample overlaps with that of CI chondrites. This points towards local Cr isotope heterogeneities within CI chondrites and Ryugu, potentially induced by aqueous alteration on their parent bodies (Yokoyama et al., 2023b). Such local heterogeneities are also indicated in elemental abundances of Ca, Sr, Mn, and rare earth elements (REE) (Nakamura et al., 2022; Yokoyama et al., 2023a). Calcium is generally enriched in the analyzed Ryugu samples compared with CI chondrites due to heterogeneously distributed carbonates formed during aqueous alteration, while enrichments in REE are attributed to the nugget effect of Ca-phosphates (Moynier et al., 2022; Yokoyama et al., 2023a). Moreover, Mo isotope data of a composite Ryugu sample indicate an *s*-process isotope depletion relative to bulk CI chondrites (Nakanishi et al., 2023). This stands in stark contrast to the identical compositions of Ryugu and CI chondrites observed for supernova-derived isotopes of Cr, Ti, and Fe (Hopp et al., 2022; Yokoyama et al., 2023a, 2023b). It is an open question whether the *s*-process depletion in Mo isotopes of Ryugu samples is a more general feature that also applies to *s*-process isotopes of other elements. This is an important topic because nucleosynthetic isotope compositions are powerful tracers for genetic relationships between planetary materials (e.g., Dauphas & Schauble, 2016; Rüfenacht et al., 2023). Identical isotopic compositions most likely reflect that either the samples originated from a single parent body or that their parent bodies accreted in the same region of the protoplanetary disk (e.g., Hopp et al., 2022; Marrocchi et al., 2023; Rüfenacht et al., 2023; Yokoyama et al., 2023a). The latter has been suggested for Ryugu and CI chondrites (e.g., Hopp et al., 2022).

Zirconium is an ideal element to address these topics. Its isotopes cover a similar mass range as Mo in the nuclide chart and thus Zr and Mo isotopes are produced by similar nucleosynthetic processes. In detail, four of the five stable Zr isotopes are predominately generated by the *s*-process (^{90}Zr, ^{91}Zr, ^{92}Zr, ^{94}Zr), while the synthesis of ^{96}Zr requires stellar environments with higher neutron fluxes, such as massive stars, supernovae explosions or neutron star mergers (for overview, see Akram et al., 2015). Limited ^{96}Zr production can also occur in intermediate-mass AGB stars (5–8 solar masses) if the ^{22}Ne source is activated (Travaglio et al., 2004). Depletions in *s*-process isotopes result in ^{96}Zr enrichments, whereas *s*-process-enriched materials display strong ^{96}Zr depletions (Akram et al., 2013, 2015; Nicolussi et al., 1997; Render et al., 2022; Schönbächler et al., 2003, 2005). Analyses of bulk solar system materials show distinct ^{96}Zr isotope variations with the Earth possessing the most *s*-process-enriched Zr isotope composition (^{96}Zr depletions) (Akram et al., 2015; Render et al., 2022). This heterogeneity has been interpreted as the result of thermal processing of dust in the solar nebula (Akram et al., 2015; Ek et al., 2020), whereby hotter temperatures close to the Sun destroyed material with solar system compositions, thereby enhancing the dominant *s*-process signal of the presolar grain fraction (Ek et al., 2020). Another study preferred the interpretation of time-varied infall from an isotopically heterogeneous molecular cloud (Nanne et al., 2019; Render et al., 2022; Yap & Tissot, 2023). Similar to the refractory and fluid immobile element Ti (Rüfenacht et al., 2023; Yokoyama et al., 2023b), evidence is missing that parent body processes such as aqueous alteration and thermal metamorphism affect the nucleosynthetic Zr isotope compositions. However, for other elements such as

Mo and Os, parent body processes might have influenced their isotopic compositions (Sanders & Scott, 2022; Yokoyama et al., 2011, 2019).

To determine the extent of *s*-process depletion in Ryugu and the origin of the materials from which Ryugu accreted, we present Zr isotope data for Ryugu samples (A0106, A0106-A0107, C0108) from the two touchdown sites. For these samples, high-precision isotope data of Mg, K, Ca, Ti, Cr, Fe, Cu, Zn, Mo, and Nd were reported previously (Bizzarro et al., 2023; Hopp et al., 2022; Hu et al., 2024; Moynier et al., 2022; Nakanishi et al., 2023; Paquet et al., 2023; Torrano et al., 2023; Yokoyama et al., 2023a, 2023b). These diverse isotopic data were all obtained from the same sample digestions and are therefore directly comparable. The Zr isotope data of Ryugu are complemented with new data from carbonaceous chondrites obtained at similar analytical conditions (Table 1) to verify our data quality. Ryugu aliquots of <25 mg were analyzed with ~40 to 70 ng Zr. This requires challenging analyses at relatively low concentrations. The Zr mass range (mass 90–96) features many molecular isobaric interferences (e.g., Fe- and Cr-argides, Ar-Ar-oxides; Schönbächler et al., 2004), that become even more of an issue for lower concentration analyses. Therefore, background and interference levels were carefully monitored and doping tests using a variety of elements were reported to assess their effect on the Zr isotope data. Besides the analytical considerations, the CI, CM, and the ungrouped C2 chondrites (Tarda and Tagish Lake) were also chosen because the global observations of Ryugu by Hayabusa 2 remote sensing showed the closest kinship to CM and CI chondrites with a low degree of hydration (Sugita et al., 2019). Hence, the sample choice allows for a comparison between Ryugu and samples from the outer solar system that might be related to D- and P-type asteroids (Schrader et al., 2024).

EXPERIMENTAL

Sample Preparation

Three samples (A0106, A0106-A0107, and C0108) from the Ryugu asteroid that were studied by Yokoyama et al. (2023a, 2023b) were measured for their Zr isotope composition. For comparison, three carbonaceous chondrites (Orgueil [CI], Murchison [CM], Allende A, and Allende B [CV]) prepared by Yokoyama et al. (2023b) were also analyzed. These samples were dissolved on a hotplate to avoid blank issues for isotope analyses of other elements (e.g., Cr; Yokoyama et al., 2023a, 2023b) carried out on these relatively small Ryugu samples (< 25 mg). In more detail, these samples and an additional 30 mg of the ungrouped carbonaceous chondrites Tagish Lake and Tarda were dissolved in concentrated HF-HNO_3 at 180°C for 3–7 days on a hotplate at the Tokyo Institute of Technology. Samples were then treated with a HNO_3-HCl mixture at 120°C for 12 h, followed by dissolution in a HNO_3-H_2O_2 mixture. In addition, 30 mg Tagish Lake (labeled high PT) and 90 mg Tarda (high PT) were digested using concentrated HF-HNO_3 in octagonal-body Savillex® vials for about a week at 220°C at Tokyo Institute of Technology. Ivuna was dissolved using two different digestion methods with 40 and 44 mg powder from a larger homogenized powder (550 mg) at ETH Zurich (Rüfenacht et al., 2023). Ivuna PB was digested with concentrated HF-HNO_3 in a Parr® bomb at 170°C following the procedures of Schönbächler et al. (2004). Ivuna high PT (termed Ivuna HP in Rüfenacht et al., 2023) was dissolved using concentrated HF-HNO_3 for 3 days, followed by digestion with concentrated HCl for 2 days in an octagonal-body Savillex® vial and oven at 160°C (see Bischoff et al., 2019). The terrestrial rock reference materials BCR-2 and AGV-1 were also digested in Parr® bombs as described above, whereas BHVO-2 was dissolved in concentrated HF-HNO_3 on a hotplate.

Zirconium was separated using a 4-step separation procedure employing anion exchange (AG 1-X8), DGA, and LN resin (Tagish Lake and Tarda: AG 1-X8 and DGA only) at the Tokyo Institute of Technology (Yokoyama et al., 2023a). For Ivuna, Zr was separated using a two-stage anion exchange separation procedure (Bio Rad resin AG 1-X8) (Rüfenacht et al., 2023; Schönbächler et al., 2004). For all samples, except Allende B, an additional separation using anion exchange resin (AG 1-X8) was employed (column 1 of Schönbächler et al., 2004 or a down-scaled version thereof) to further decrease Mo levels in the Zr fractions. Additionally, Zr was separated from terrestrial samples (BHVO-2, BCR-2, AGV-1) using a three-stage separation procedure employing AG 1-X8 and LN resin (Scheme B, Iizuka et al., 2016).

Total procedural blanks prepared together with Tarda and Tagish Lake contained 0.08 and 0.24 ng Zr, while total blanks treated alongside Ivuna were 0.09 and 0.13 ng Zr. For Orgueil and Murchison, a similar amount of Zr (30–36 ng) was recovered as for the Ryugu samples (30–50 ng), which corresponds to a maximum blank contribution of 0.8%. All other samples contain larger Zr amounts and therefore have negligible blank contribution.

For comparison, Zr fractions of terrestrial rock reference materials (BHVO-2, SCo-1), eucrites (Bouvante and Bereba), and the carbonaceous chondrite Colony (CO) from Akram et al. (2015) were re-measured. These samples were digested using Parr® bombs and Zr was separated using the two-stage anion exchange separation procedure of Schönbächler et al. (2004).

TABLE 1. Zr isotope data for geological samples.

Sample name	Group, sample details	ppb Zr[a]	*n*	$\varepsilon^{91}Zr$	2SD	2SE	$\varepsilon^{92}Zr$	2SD	2SE	$\varepsilon^{96}Zr_{99corr}$	2SD	2SE	$\varepsilon^{96}Zr_{101corr}$	2SD	2SE
Ryugu															
A0106-A0107	Ryugu, Hayabusa 2	30	1	−0.21	0.26		−0.22	0.23		2.8	1.0		2.9	1.0	
A0106	Ryugu, Hayabusa 2	30	2	n.d.			0.27	0.23		2.3	1.0		2.4	1.0	
C0108	Ryugu, Hayabusa 2	16.7, 30	3	0.14	0.26		0.06	0.23		2.1	1.0		2.2	1.0	
Average Ryugu—all individual analyses	Ryugu, Hayabusa 2	16.7, 30	4, 6	0.06	0.26	0.18	0.08	0.43	0.17	2.3	0.8	0.3	2.4	0.8	0.3
Average Ryugu—samples	Ryugu, Hayabusa 2	16.7, 30	2, 3	−0.03	0.26		0.04	0.23		2.4	1.0		2.5	1.0	
Carbonaceous chondrites															
Ivuna high PT[b]	CI	30	5	0.03	0.05	0.02	−0.09	0.27	0.12	0.49	0.59	0.26	0.43	0.72	0.32
Ivuna PB	CI	30	6	−0.09	0.38	0.16	0.03	0.18	0.07	1.14	1.90	0.78	1.16	1.82	0.74
Orgueil	CI	16.7, 30	3	n.d.			0.17	0.23		1.2	1.0		1.2	1.0	
Tagish Lake high PT	C-ungrouped	30	6	−0.06	0.16	0.07	0.03	0.23	0.10	1.52	1.25	0.51	1.52	1.18	0.48
Tagish Lake HP	C-ungrouped	30	8	0.03	0.18	0.06	0.08	0.24	0.08	0.82	1.04	0.37	0.87	1.09	0.38
Tarda high PT	C-ungrouped	30	11	−0.01	0.38	0.11	0.04	0.13	0.04	1.30	0.53	0.16	1.27	0.53	0.16
Tarda HP	C-ungrouped	30	7	−0.02	0.16	0.06	0.10	0.29	0.11	2.11	0.95	0.36	2.08	0.92	0.35
Murchison	CM2	30	2	0.16	0.26		0.24	0.23		0.6	1.0		0.6	1.0	
Colony	CO3, BM 1984 M4	30	38	−0.02	0.26	0.04	−0.05	0.23	0.04	0.87	0.99	0.16	0.88	0.98	0.16
Allende A	CV3	30	5	0.02	0.22	0.10	0.04	0.36	0.16	1.20	0.55	0.25	1.15	0.57	0.25
Allende B	CV3	30, 60	8	0.09	0.30	0.11	0.05	0.23	0.08	0.96	0.69	0.24	1.01	0.71	0.25
Average Allende	CV3	30, 60	12	0.04	0.23	0.07	0.05	0.28	0.08	1.11	0.55	0.16	1.12	0.54	0.16
Eucrites															
Bouvante	Eucrite, (PE) 3223 MS	30, 60	36	−0.04	0.31	0.05	−0.01	0.30	0.05	0.71	0.79	0.13	0.71	0.83	0.14
Bereba	Eucrite, PE 1297C MS	30	17	−0.12	0.23	0.06	−0.01	0.25	0.06	0.50	0.76	0.19	0.49	0.80	0.19
Terrestrial reference rocks															
AGV-1	Andesite, Oregon	30	75	0.07	0.25	0.03	0.06	0.23	0.03	−0.18	1.05	0.12	−0.17	1.05	0.12
BCR-2	Basalt, Columbia River	30	99	0.07	0.26	0.03	0.06	0.23	0.02	−0.10	0.91	0.09	−0.10	0.93	0.09
BHVO2 (a)	Basalt, Hawaii	30, 60	80	−0.01	0.28	0.03	−0.02	0.21	0.02	0.22	1.12	0.13	0.22	1.09	0.12
BHVO2 (b)	Basalt, Hawaii	30, 60	13	−0.03	0.29	0.08	0.02	0.20	0.06	0.25	1.22	0.34	0.22	1.20	0.33
Average BHVO-2	Basalt, Hawaii	30, 60	92	−0.02	0.27	0.03	−0.02	0.21	0.02	0.23	1.12	0.12	0.22	1.10	0.11
SCo-1, Cody Shale	Shale, Wyoming	30, 60	86	0.02	0.27	0.03	−0.02	0.22	0.02	0.14	1.19	0.13	0.15	1.18	0.13

Note: An outlier rejection was carried out with rejection of data that falls outside the 2SD uncertainty. For samples with $n < 5$, the 2SD of Colony is displayed as the uncertainty. *n* refers to number of measurements. $\varepsilon^{96}Zr_{99corr}$ or $\varepsilon^{96}Zr_{101corr}$ refers to the Ru interference correction using ^{99}Ru or ^{101}Ru, respectively.

Abbreviation: n.d., not determined.

[a]ppb Zr refers to the concentration of the analyzed solution.

[b]Termed Ivuna HP in Rüfenacht et al. (2023).

Mass Spectrometry

Zirconium isotope compositions were measured on a Thermo Scientific Neptune Plus multi-collector inductively coupled plasma mass spectrometer (MC-ICP-MS) at ETH Zurich. Normal skimmer and sampler cones were utilized. Sample introduction employed an Aridus II desolvating nebulizer system and a PFA nebulizer with an approximate uptake rate of 0.05 mL/min. Faraday cups with 10^{11} Ω amplifiers were used to collect Zr masses ^{90}Zr to ^{96}Zr and ^{95}Mo, whereas 10^{12} Ω amplifiers were applied for the collection of ^{99}Ru and ^{101}Ru. Zirconium isotope measurements of standards, samples, and backgrounds included the static collection of 60 ratios with an integration time of 4.2 s. Electronic baselines were measured for 30 s prior to each analysis. An on-peak background correction was performed. Samples and standards were measured in 0.5 M HNO_3–0.005 M HF at 30 ppb Zr. One sample analysis at 30 ppb generally consumed 15 ng Zr. A few additional analyses were performed at 17 and 60 ppb Zr. Total Zr ion beams ranged from 3.5 to 13 V. Tuning was performed to minimize interferences of $^{40}Ar_2{}^{16}O^+$ and $^{40}Ar_2{}^{14}N^+$ on $^{96}Zr^+$ and $^{94}Zr^+$ and with it the on-peak background corrections. Background corrections were on average 0.3, 2, and 98 ppm for $^{91}Zr/^{90}Zr$, $^{92}Zr/^{90}Zr$, and $^{96}Zr/^{90}Zr$, respectively. For most analyses (all carbonaceous chondrites except Colony), backgrounds were ≤12 ppm for $^{91}Zr/^{90}Zr$, ≤22 ppm for $^{92}Zr/^{90}Zr$, and ≤175 ppm for $^{96}Zr/^{90}Zr$, whereas background corrections were up to 20 ppm for $^{91}Zr/^{90}Zr$, 36 ppm $^{92}Zr/^{90}Zr$, and 730 ppm $^{96}Zr/^{90}Zr$ for a few analyses of Colony, eucrites and terrestrial samples. Molybdenum and Ru corrections were calculated using the signals on mass 95 (^{95}Mo), 99 (^{99}Ru), and 101 (^{101}Ru). An initial Mo correction utilized a mass bias correction relative to $^{91}Zr/^{90}Zr = 0.21798$ (Minster & Ricard, 1981) as detailed in Schönbächler et al. (2004). Zirconium isotope data are internally normalized to a $^{94}Zr/^{90}Zr$ ratio of 0.3381 (Minster & Ricard, 1981) using the exponential law to correct for mass bias. The Zr isotope results are reported relative to the NIST SRM 3169 Zr standard using the standard sample bracketing method:

$$\varepsilon^{x/90}\mathrm{Zr} = \left(\frac{{}^{x}\mathrm{Zr}/{}^{90}\mathrm{Zr}_{\mathrm{sample}}}{{}^{x}\mathrm{Zr}/{}^{90}\mathrm{Zr}_{\mathrm{NIST\ SRM\ 3169}}} - 1\right) \times 10^4 \quad (1)$$

with $x = 91$, 92 and 96.

Ruthenium interference correction based on ^{99}Ru and ^{101}Ru yielded consistent results (Table 1). The ε^{96}Zr data in the main text refers to the data corrected using ^{99}Ru. The purity of samples was checked prior to analyses on a Thermo Scientific Element XR ICPMS and Neptune MC-ICP-MS. The Mo/Zr and Ru/Zr ratios were ≤0.0007 and <0.00005, respectively, for all analyzed samples. The Hf/Zr ratios were ≤0.0025 for samples after the LN-separation step, whereas these ratios were between 0.021 and 0.033 for Tagish Lake, Tarda, Ivuna, and samples from Akram et al. (2015). The effect of remaining trace impurities in the purified Zr sample fractions was assessed by comparison of known versus unknown samples and doping tests (see Supplementary Material). Doping tests were performed for remaining impurities present at trace levels in the Zr fractions. They include Ti, V, Cr, Mo, Hf, and W. The results show that the observed trace levels have no effect on the accuracy of the Zr isotope data.

RESULTS

Precision and Accuracy of Standard Solutions

The Zr standard material NIST SRM 3169 was analyzed in each session. For low concentration analyses at 30 ppb, the external precision expressed as 2 standard deviations (2SD) for an average session ($n = 32$; $n =$ a number of measurements) was 0.35, 0.21, and 1.00 for ε^{91}Zr, ε^{92}Zr, and ε^{96}Zr, respectively. For Zr isotope analyses at 350 ppb, these values improved to 0.08, 0.07, and 0.26 for ε^{91}Zr, ε^{92}Zr, and ε^{96}Zr ($n = 37$) (Tissot et al., 2023).

Precision and Accuracy of Sample Measurements for Low-Concentration Analyses

The terrestrial rock reference materials BHVO-2, BCR-2, AGV-1 and SCo-1 were analyzed many times over the course of this study (10 months, $n = 13$–99; Table 1 and Table S2, Figure 1). In addition, the eucrites Bouvante and Bereba, as well as the CO chondrite Colony, were also frequently analyzed ($n = 17$–38; Table 1 and Table S3). The external reproducibility (2SD) only varied little for the different samples with average values of 0.3, 0.2, and 1.0 for ε^{91}Zr, ε^{92}Zr, and ε^{96}Zr, respectively. These values are very similar to those of pure standard solutions at 30 ppb. The external precision estimated from the geological sample measurements integrates the uncertainty introduced by the chemical separation procedure and mass spectrometry. The Zr isotope composition of the terrestrial samples is zero by definition because (i) the data are given in epsilon notation relative to the terrestrial Zr NIST SRM 3169 standard (Equation 1) and (ii) previous studies showed that the Zr NIST SRM 3169 standard has an identical Zr isotope composition to terrestrial rock reference materials (e.g., Tissot et al., 2023). Considering the 2SD, all terrestrial samples overlap with zero for ε^{91}Zr, ε^{92}Zr, and ε^{96}Zr, indicating that our data are accurate. Considering the 2 standard error (2SE), the Zr isotope composition is

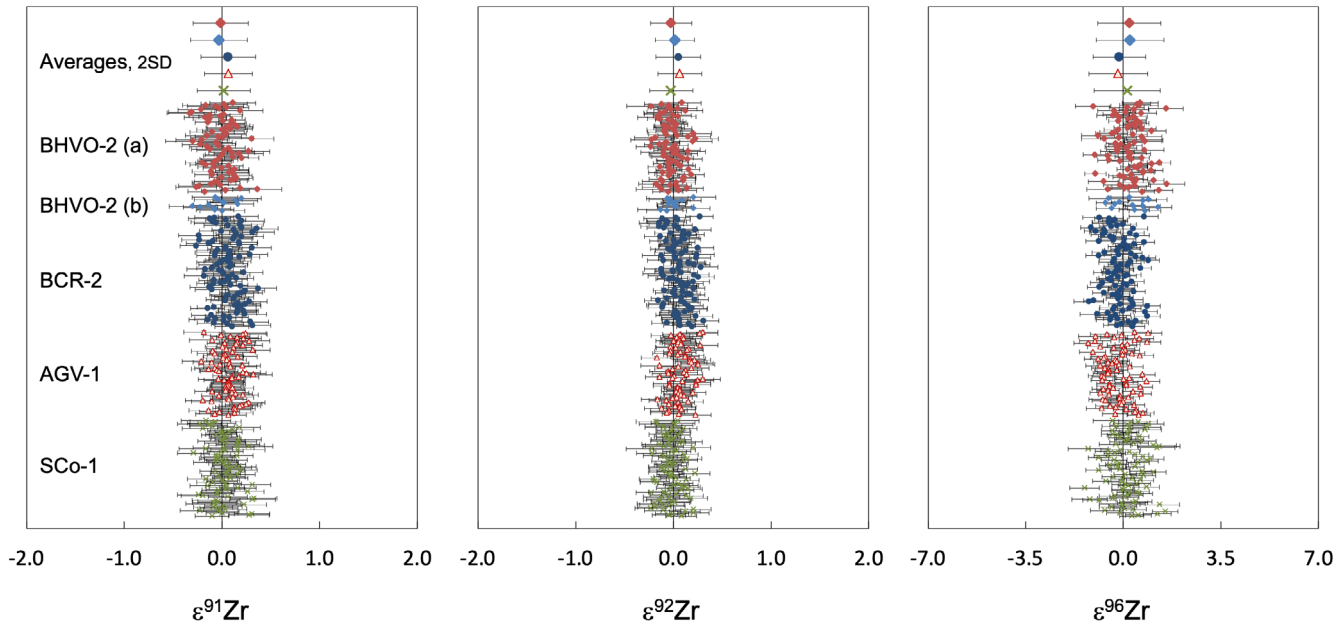

FIGURE 1. The Zr isotope data for five terrestrial rock reference materials. BHVO-2 (a) and (b) denote two different digestions. Shown are single measurements and their internal error (2SE) as well as the average of each sample with the corresponding uncertainty given as the 2 sd calculated from the individual sample measurements (Table 1 and Table S2). For ε^{96}Zr, values using ^{99}Ru for Ru interference correction are shown.

not always zero if n is large (e.g., $n = 75$ and 99 for AGV-1 and BCR-2). For example, AGV-1 yields an average and 2SE values of 0.07 ± 0.03, 0.06 ± 0.03, and -0.18 ± 0.12 for ε^{91}Zr, ε^{92}Zr and ε^{96}Zr, respectively (Table 1). Hence, in particular, if n is large, the 2SE sometimes slightly underestimates the true analytical uncertainties. The pattern observed is within the analytical uncertainties of the Ryugu samples and shows positive ε^{91}Zr, ε^{92}Zr (<0.07 ε), and negative ε^{96}Zr values (<0.18 ε). This matches the expected signature if the mass bias does not fully follow the exponential law (Akram & Schönbächler, 2016; Tissot et al., 2023). On the other hand, this pattern is not observed for BHVO-2 and Cody Shale, which include analyses at higher signal sizes. This indicates an underlying potential interference issue, which is not relevant to the precision of the reported data.

The accuracy of the Zr isotope data is also demonstrated by the analyzed meteorites. The Zr isotope data of Bouvante, Bereba and Colony overlap with previously reported values within reported uncertainties (Figure 2). In addition, several meteorites (Allende A, B, Orgueil, Murchison) were processed alongside the Ryugu samples and the results overlap with literature values (Figure 2). This demonstrates the accuracy of our data.

Results for Carbonaceous Chondrites and Ryugu Samples

Our Zr isotope data for the Ryugu samples from the two touchdown sites yield identical compositions (first touchdown: A0106, A0106-A0107; second touchdown: C0108) (Table 1). This is in line with nucleosynthetic isotope data from Ti, Fe, and Zn (Hopp et al., 2022; Paquet et al., 2023; Yokoyama et al., 2023a, 2023b). Like the Zr isotope data of carbonaceous chondrites, the average Zr isotope composition of the Ryugu samples reveals an ε^{96}Zr excess relative to Earth of 2.3 ± 0.3 (2SE) (Figure 3, Table 1). However, Ryugu data are generally higher in ε^{96}Zr (by ~1–1.5ε) compared with CI chondrites.

DISCUSSION

The ε^{96}Zr excess for Ryugu samples relative to CI chondrites shows that Ryugu samples are more depleted in *s*-process Zr relative to Earth than any known chondrite group. This could be (i) a true feature of the bulk asteroid Ryugu, (ii) due to heterogeneities or incomplete digestion of presolar silicon carbide (SiC), which are mainly of *s*-process origin (low ε^{96}Zr) (Zinner, 2014), or (iii) sample heterogeneity of an *s*-process depleted phase (high ε^{96}Zr). These options are discussed in the following.

Bulk Composition of Asteroid Ryugu

Taking the data at face value suggests that the bulk composition of the asteroid Ryugu is characterized by a larger *s*-process deficit in Zr isotopes than any analyzed bulk chondrite group from our collections. In line with

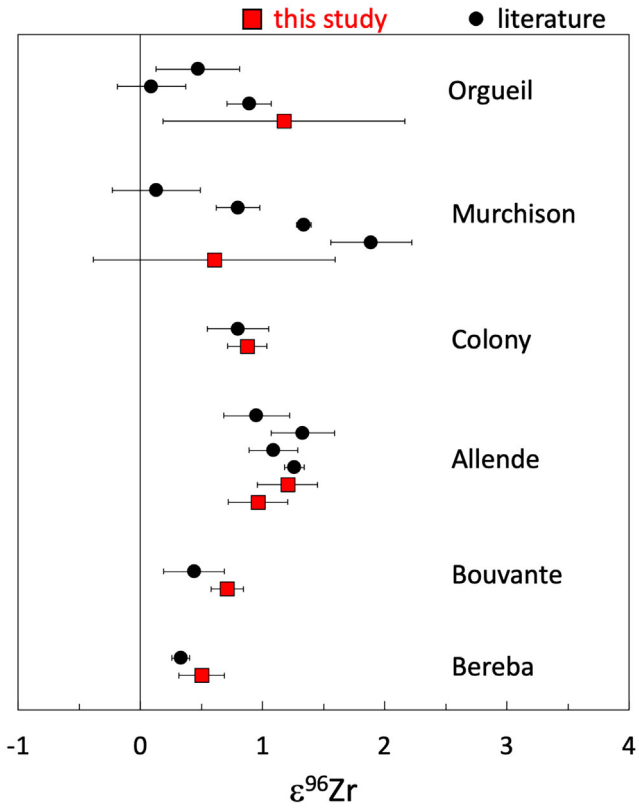

FIGURE 2. The ε^{96}Zr data for several meteorites. Data are from Table 1 using ε^{96}Zr $_{(99\ corr.)}$ and from Akram et al. (2013, 2015); Elfers et al. (2020); Render and Brennecka (2021); Render et al. (2022). The data of Akram et al. (2013, 2015), originally analyzed against an Alfa Aesar Zr standard, were recalculated relative to NIST SRM 3169 Zr using the values from Akram and Schönbächler (2016). Uncertainties are given as 2SE for data from this study and as 95% CI for data from Render and Brennecka (2021) and Render et al. (2022), except if $n < 5$, where the 2SD of Colony is used (±1) for data from this study and published 2SD for literature data.

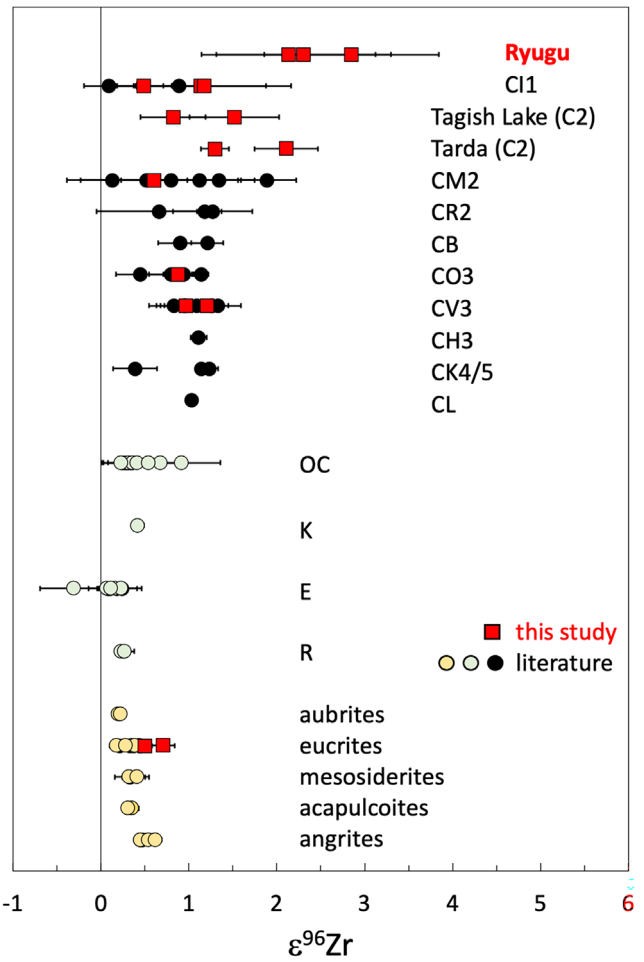

FIGURE 3. The ε^{96}Zr data for bulk samples of Ryugu and various meteorite groups. The spread in the data is generally larger for meteorite groups that experienced higher degrees of aqueous alteration (types 1 and 2) compared with those with less alteration (e.g., CV3). Red symbols denote data from this study (Table 1 using ε^{96}Zr $_{(99\ corr.)}$). Literature data are from the compilation published in Rüfenacht et al. (2023), summarizing results from Akram et al. (2013, 2015); Elfers et al. (2020); Render and Brennecka (2021); Render et al. (2022). Uncertainties are the same as in Figure 2.

Zr, the Mo isotope data obtained on the same sample digestions of Ryugu also indicates an increased *s*-process depletion (Nakanishi et al., 2023). In contrast, Ryugu and CI chondrites share strong similarities in chemical and O isotope compositions (Nakamura et al., 2022; Yokoyama et al., 2023a). They also display identical nucleosynthetic Ti, Fe, and Zn isotope compositions, indicating that Ryugu and CI chondrites accreted in the same region of the outer protoplanetary disk (Hopp et al., 2022; Paquet et al., 2023; Yokoyama et al., 2023a, 2023b), although Mg isotope data hint at potential heterogeneities (Bizzarro et al., 2023). In addition, the Cr isotope data overlaps with the range of composition obtained for CI chondrites, with some local variation between the different Ryugu samples, most likely due to parent body processing during aqueous alteration (Yokoyama et al., 2023b). It is also noteworthy that the size of the analyzed Ryugu samples is small (<25 mg each) and this increases the likelihood that the samples are not representative of the bulk composition of the asteroid Ryugu (Yokoyama et al., 2023b). In summary, it is considered unlikely that bulk Ryugu has a unique Zr and Mo isotope composition because of the wealth of evidence for a strong genetic relationship between Ryugu and CI chondrites and the small sample sizes analyzed.

Incomplete Digestion Effects

Incomplete digestion can induce apparent local heterogeneities during the analytical processing of

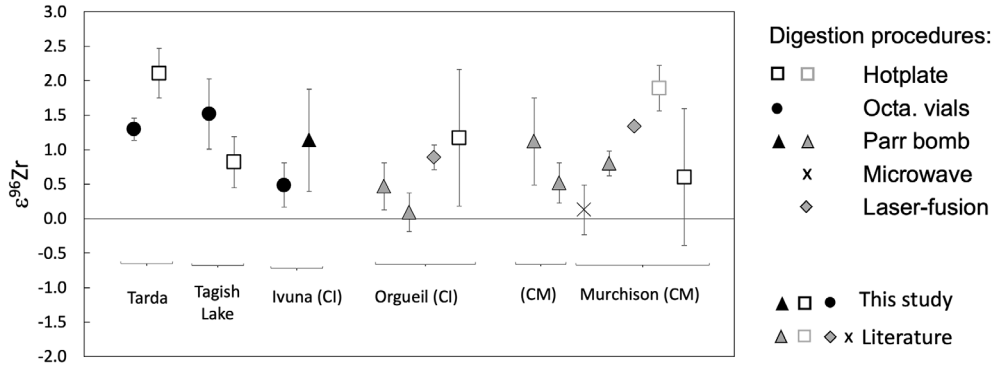

FIGURE 4. Comparisons of Zr isotope data of carbonaceous chondrites analyzed using different digestion methods during sample preparation. Uncertainties and data sources are the same as in Figure 2. Octa: octagonal-body Savillex® vials.

TABLE 2. Values for mass balance calculations.

Sample	Concentration	Error	Zr	Mo	Reference
Presolar SiC					
Ryugu	25 ppm	+6/−5			Barosch et al. (2022)
	45 ppm	+12/−10			Nguyen et al. (2023)
Ryugu (average)	35 ppm				
Orgueil (CI1)	34 ppm	+11/−8			Davidson et al. (2014), Huss and Lewis (1995)[a]
Murchison (CM2)	9 ppm	+4/−3			Davidson et al. (2014), Huss and Lewis (1995)[a]
Element concentration					
SiC (average)			97 ppm	43 ppm	Kashiv et al. (2001, 2010); Amari et al. (1995)
Bulk Ryugu			4 ppm	1 ppm	Nakamura et al. (2022), Yokoyama et al. (2023a)
Bulk Orgueil (CI1)			3.79 ppm	0.976 ppm	Lodders (2021)
Average isotope composition of SiC grains[b]					
$d^{90}Zr$			−102		Nicolussi et al. (1997)
$d^{91}Zr$			−66		
$d^{92}Zr$			−42		
$d^{96}Zr$			−551		
$d^{92}Mo$				−686	Liu et al. (2019); Stephan et al. (2019)
$d^{94}Mo$				−662	
$d^{95}Mo$				−418	
$d^{97}Mo$				−356	
$d^{98}Mo$				−167	
$d^{100}Mo$				−671	

Note: $\delta^{x}Zr = [(^{x}Zr/^{94}Zr)/(^{x}Zr/^{94}Zr)_{solar} - 1] \times 1000$, where $x = 90, 91, 92, 96$. $\delta^{x}Mo = [(^{x}Mo/^{96}Mo)/(^{x}Mo/^{96}Mo)_{solar} - 1] \times 1000$, where $x = 92, 94, 95, 97, 98, 100$.

[a]Values used for the calculations are from Davidson et al. (2014), but overlap with those of Huss and Lewis (1995). Davidson et al. (2014) values are chosen because they were determined by the same technique as those from Barosch et al. (2022) for Ryugu.

[b]These values are for mainstream SiC grains. Taking SiC X grains into account in addition to mainstream SiC does not affect the conclusions of this study. Mass balance calculations were carried out to determine the average isotopic composition of SiC grains in carbonaceous chondrites as a mixture of SiC X and mainstream grains. These calculations used the abundances of SiC X and mainstream grains in carbonaceous chondrites from Stephan et al. (2024) and the Mo and Zr isotope composition of X grains from Pellin et al. (2006). The Zr and Mo concentrations in X grain are not well known, thus it was assumed that the concentrations are identical in both grain types.

chondrite samples. Ryugu samples were dissolved on a hotplate (HP). Previous work showed that HP digestions can lead to elevated $\varepsilon^{96}Zr$ values due to incomplete digestion of presolar SiC grains, which carry *s*-process Zr with strong ^{96}Zr depletions (Akram et al., 2013). To test this effect further, Tarda and Tagish Lake powders were subjected to two different digestion procedures: an HP digestion and a more rigorous digestion in octagonal-body Savillex® vials (here labeled as high PT). For Tarda, the HP digestion yields an elevated $\varepsilon^{96}Zr$ of 2.11 ± 0.36 compared with the high-PT digestion with 1.30 ± 0.16, while the data of the two Tagish Lake digestions overlap within analytical uncertainty (Figure 4, Table 1). This is reminiscent of data for HP and Parr® bomb digestions of the CM chondrite Murchison, with $\varepsilon^{96}Zr$ values of 1.9 ± 0.3 and 0.8 ± 0.2, respectively

(Akram et al., 2013) and hints at incomplete digestion of presolar SiC grains. Moreover, two aliquots of an Ivuna powder dissolved by Parr® bomb and high-PT digestion with octagonal-body vials show identical ε^{96}Zr compositions within the reported analytical uncertainties (Figure 4, Table 1). This indicates that high-PT digestions in octagonal-body vials are as effective as the more aggressive Parr® bomb digestion for low-concentration Zr isotope analyses. In contrast, HP digestions may not always yield the true bulk Zr isotope composition, but instead artificially elevated ε^{96}Zr values. Relatively, high-precision analyses are required (<0.5 ε for ε^{96}Zr) to resolve the HP digestion effect. This is at the limit of the resolution with the precision of the current study. Hence, the results leave room for interpretation. Nevertheless, the data show that it is paramount for Zr isotope analyses to use a more aggressive sample digestion procedure than an HP digestion to avoid the risk of incomplete digestion.

Leach experiments performed on Orgueil (CI1) indicate that ε^{96}Zr excesses for HP-digested aliquots may stem from the incomplete digestion of SiC grains. Orgueil powder was subjected to progressively stronger acid leaching and the final Parr® bomb digestion revealed a strong SiC signal ($\varepsilon^{96}Zr = -377.5 \pm 3.3$; Schönbächler et al., 2005). This is supported by mass balance consideration. For example, mass balance calculation based on the values given in Table 2 shows that the dissolution of about 45% of the SiC grains in the Ryugu samples (leaving the rest undissolved) shifts the average CI value (0.65 ± 0.38, Rüfenacht et al., 2023) to the observed ε^{96}Zr average value of Ryugu (Table 1). Since presolar SiC grains are also significant carriers of *s*-process Mo, analogous calculations were carried out for Mo. Using an average Mo abundance of 42.8 ppm for presolar SiC grains (Kashiv et al., 2001) and the parameters from Table 2 for the mass balance calculation results in roughly 25% of the SiC grains being undissolved in the Ryugu samples. There is good agreement between the Zr and Mo results, considering the large uncertainties in these estimates (e.g., Mo concentration in SiC grains is uncertain up by a factor of 100, while Zr data converges to 97 ± 27 ppm; Amari et al., 1995; Kashiv et al., 2001, 2010). This agreement indicates that incomplete digestion may be a potential explanation for the *s*-process enrichment of Ryugu for Zr and Mo isotopes.

Sample Heterogeneity

Sample heterogeneity within Ryugu samples is another possible reason for the observed *s*-process depletion. For example, calcium-aluminum-rich inclusions (CAI) exhibit ε^{96}Zr excesses (Akram et al., 2013; Schönbächler et al., 2003). However, to explain the elevated ε^{96}Zr data of Ryugu compared with CI chondrites, the Ryugu samples must contain more refractory inclusions than Allende (CV3). Such high-CAI abundances would manifest itself in the elemental abundances, which are not observed (Nakamura et al., 2022; Nakashima et al., 2023). Even considering that amoeboid olivine aggregates might have a CAI-like Zr isotope composition (no Zr data available) as demonstrated for Ti and Cr isotopes (Jansen et al., 2024; Torrano et al., 2024), higher enrichments than in Allende are not indicated for the Ryugu samples (Nakamura et al., 2022; Nakashima et al., 2023).

Strikingly, the dispersion of the Zr isotope data increases in meteorite classes that experienced higher degrees of aqueous alteration (CI1, CM2, CR2, C2) (Figure 3). This indicates heterogeneities that might be due to (i) fluids during aqueous alteration moving and depleting presolar SiC grains in the analyzed small Ryugu aliquots by 30%–50% (numbers from mass balance calculations) or (ii) that aqueous alteration dissolved a labile presolar phase with ^{96}Zr excesses and heterogeneously redistributed it. It is not possible to fully exclude that a true heterogeneity in presolar SiC caused the ε^{96}Zr enrichment. However, the SiC abundance of Ryugu was estimated from a relatively small total area of ~39,000 μm^2 (Barosch et al., 2022) and 32,435 μm^2 (Nguyen et al., 2023) in thin sections and pressed particles. The resulting abundances are $25 + 6/-5$ ppm and $45 + 12/-10$ ppm, respectively, and overlap with that of the CI chondrite Orgueil ($34 + 11/-8$ ppm; Davidson et al., 2014). This provides evidence for very similar SiC abundances in CI chondrites and Ryugu. We thus consider a true heterogeneity of SiC less likely than effects from incomplete dissolutions, although the errors allow for a ~10 ppm difference in SiC abundances, which is already almost sufficient to cause the observed ε^{96}Zr enrichment in Ryugu samples.

Interestingly, Nguyen et al. (2023) reported extremely high-SiC abundances of ~235 ppm in primitive clasts in Ryugu samples. Such clasts are rare and of exogenous origin. They also escaped aqueous alteration. Excessive enrichments of presolar SiC in Ryugu, however, cannot explain the observed *s*-process depleted signature, because it would induce excesses, leading to lower ε^{96}Zr values.

It is also possible that aqueous alteration dissolved a susceptible presolar phase with ^{96}Zr excesses, followed by Zr precipitation from the fluid into a phase newly formed during aqueous alteration. This phase was heterogeneously distributed in Ryugu to generate the measured *s*-process isotope depletion. Leaching experiments of carbonaceous chondrites reveals that the first mild leachates, dissolving easily leachable phases (e.g., carbonates, sulfates) formed by aqueous alteration, display positive ε^{96}Zr values (Elfers et al., 2020; Render et al., 2022; Schönbächler et al., 2005). For example, acetic

acid leachates of Murchison from three different leaching experiments yield ε^{96}Zr values of 48.6 ± 1.4, 44.9 ± 1.4, and 49.98 ± 0.18 (Render et al., 2022; Schönbächler et al., 2005). Acetic acid is unlikely to attack refractory SiC grains. Mass balance calculation based on Table 2 shows that not dissolving any SiC grains from Murchison would shift its ε^{96}Zr values by +0.65 and +7.3, assuming an average Zr content of SiC of 90 ppm or an absolute maximum of 1000 ppm (Amari et al., 1995; Kashiv et al., 2001, 2010), respectively. Hence, acid resistant SiC cannot account for the extreme positive ε^{96}Zr values of +45 to +50 in these acetic acid leachates. This observation entails the presence of additional carriers of anomalous Zr. Part of this positive shift could be due to presolar silicates with an *s*-process signature (Schönbächler et al., 2005), however, Zr isotope and abundance data are missing for presolar silicates to verify this idea. Therefore, it is conceivable that the acetic acid leachates sampled a nucleosynthetic component characterized by excess ^{96}Zr, that has been mobilized and precipitated during aqueous alteration. The carrier phases of such excess ^{96}Zr in Ryugu could be carbonates because relative to the CI chondrites, Ryugu samples measured so far are enriched in elements (e.g., Ca, Sr, and Mn) that are abundant in carbonates formed by aqueous alteration (Moynier et al., 2022; Yokoyama et al., 2023a, 2023b). Noteworthy, in the leaching experiment of the CI chondrite Orgueil, only little Zr is released in the acetic acid fraction aimed at dissolving carbonates (0.44% of the total Zr; Schönbächler et al., 2005), while 33% is released in the next stronger digestion step with HNO_3. This HNO_3 step will attack Ca-phosphates and phyllosilicates, both of which are enriched in Zr in Ryugu relative to its bulk abundance (Nakamura et al., 2022). Moreover, Ryugu samples show elevated REE abundances relative to CI and they vary due to the heterogenous distribution of REE-rich Ca-phosphate grains (Yokoyama et al., 2023a). Hence, if we accept an aqueously altered carrier phase with excess ^{96}Zr, Ca-phosphates or phyllosilicates might be potential carrier phases.

Ryugu samples show *s*-process depletions in both Mo (Nakanishi et al., 2023) and Zr (Table 1, Figure 3). It is noteworthy that Mo isotope analyses of leachates from carbonaceous chondrites also exhibit *s*-process depletions in the first leaching steps (Burkhardt et al., 2012; Dauphas et al., 2002), which indicates that aqueous alteration might have led to the *s*-process depletion observed in the Ryugu samples. Neutron-rich Ti isotopes, which are produced in a supernova environment, do not show a strongly anomalous signature in the first leaching steps (Trinquier et al., 2009) and in line with this, no excesses relative to CI chondrites are observed. Neutron-rich Cr isotopes, however, are depleted in the first leaching steps of Ivuna (Schiller et al., 2014), indicating that they are affected by aqueous alteration, in agreement with the observed local variations between Ryugu samples (Yokoyama et al., 2023b). The different behavior of Zr and Mo versus Ti and Cr emphasizes that the original carriers of these nucleosynthetic signatures are distinct. Furthermore, it follows from the mixing equations, that the proportion of an element abundance in anomalous presolar phases relative to that in average solar system material is important. An element abundant in solar system materials will require higher amounts of isotopically anomalous material to generate distinct and measurable differences, assuming similar isotopic differences between solar system material and an anomalous presolar phase. This is another striking difference between the relatively abundant elements Cr and Ti and elements that are generally at trace levels in solar system materials such as Zr and Mo.

Therefore, leaching experiments are consistent with an aqueous alteration phase that is depleted in *s*-process Mo and Zr, but does not carry significant anomalies in the supernova-derived isotopes of Ti and a depletion in ^{54}Cr. However, so far no aqueous alteration phase with *s*-process depletion has been identified by in situ analyses. Moreover, Murchison shows one of the most extreme *s*-process depleted signatures of all bulk chondrites for Mo isotopes (Burkhardt et al., 2011), whereas ε^{96}Zr and Ru isotope data of Murchison fall well within the range defined by carbonaceous chondrites (Akram et al., 2015; Fischer-Gödde et al., 2015; Render et al., 2022). Since Murchison has experienced significant aqueous alteration, this indicates that aqueous alteration mobilizes Mo more easily than the refractory elements Zr or Ru and thus Mo can be decoupled from Zr and Ru.

In summary, the *s*-process depletion in Mo and Zr isotopes of Ryugu samples most likely reflects (i) incomplete dissolution of presolar SiC, (ii) depletion of SiC grain on a local scale, or (iii) enrichment of a phase carrying an *s*-process depletion that formed during aqueous alteration. It is currently impossible to firmly exclude any of these options.

CONCLUSIONS

We report Zr isotope data for three Ryugu samples (A0106, A0106-A0107, and C0108). Due to the limited availability of the sample material, low-concentration analyses were necessary. To verify the accuracy and precision of the data, we report a large data set of Zr isotope analyses for terrestrial rock reference materials (BHVO-2, BCR-2, AGV-1, and SCo-1) analyzed at similar conditions as the Ryugu samples. In addition, a set of eucrites and carbonaceous chondrites were analyzed. Both groups are enriched in ε^{96}Zr relative to Earth indicating a depletion in *s*-process material, in agreement with previous

studies (Akram et al., 2013, 2015; Render et al., 2022; Render & Brennecka, 2021). Ryugu samples yield an average ε^{96}Zr value of 2.3 ± 0.3 and are slightly enriched in ε^{96}Zr relative to CI chondrites and other carbonaceous chondrites. This reveals an *s*-process depletion in Zr isotopes similar to that of Mo in Ryugu samples (Nakanishi et al., 2023). In contrast, Ti, Cr, and Fe isotope compositions, which are dominated by supernovae contributions, overlap well with that of CI chondrites. The observed *s*-process depletion is unlikely a feature of the bulk asteroid Ryugu, but could originate from (i) incomplete digestion of SiC grains that carry an *s*-process signature, (ii) depletion of SiC grains in the analyzed samples, or (iii) the presence of an *s*-process depleted component, which was originally hosted in a labile phase that was dissolved during aqueous alteration and precipitated into heterogeneously distributed secondary phases such as phyllosilicate or Ca-phosphates.

Acknowledgments—This work has been carried out under the Hayabusa 2 Initial Analysis Team. We are grateful to Yi-Jen Lai and Waheed Akram for providing Zr fractions of terrestrial samples, eucrites, and Colony. MF and MS thank Katarzyna Liszewska, Précillia Morino, and Miriam Rüfenacht for help with the sample preparation of Ivuna and Miriam Rüfenacht and Mattias Ek for providing a summary of Zr isotope literature data. This work (MS) has partially been carried out within the framework of the NCCR PlanetS supported by the Swiss NSF under grant 51NF40_205606. Open access funding provided by Eidgenossische Technische Hochschule Zurich.

Data Availability Statement—Data available in article supplementary material.

Editorial Handling—Dr. Yves Marrocchi

REFERENCES

Akram, W., and Schönbächler, M. 2016. Zirconium Isotope Constraints on the Composition of Theia and Current Moon-Forming Theories. *Earth and Planetary Science Letters* 449: 302–310.

Akram, W., Schönbächler, M., Bisterzo, S., and Gallino, R. 2015. Zirconium Isotope Evidence for the Heterogeneous Distribution of s–Process Materials in the Solar System. *Geochimica et Cosmochimica Acta* 165: 484–500.

Akram, W., Schönbächler, M., Sprung, P., and Vogel, N. 2013. Zirconium—Hafnium Isotope Evidence from Meteorites for the Decoupled Synthesis of Light and Heavy Neutron-Rich Nuclei. *The Astrophysical Journal* 777: 169.

Amari, S., Hoppe, P., Zinner, E., and Lewis, R. S. 1995. Trace-Element Concentrations in Single Circumstellar Silicon Carbide Grains from the Murchison Meteorite. *Meteoritics* 30: 679–693.

Barosch, J., Nittler, L. R., Wang, J., Alexander, C. M. D., De Gregorio, B. T., Engrand, C., Kebukawa, Y., et al. 2022. Presolar Stardust in Asteroid Ryugu. *The Astrophysical Journal Letters* 935: L3.

Bischoff, A., Barrat, J.-A., Berndt, J., Borovicka, J., Burkhardt, C., Busemann, H., Hakenmüller, J., et al. 2019. The Renchen L5-6 Chondrite Breccia—The First Confirmed Meteorite Fall from Baden-Württemberg (Germany). *Geochemistry* 79: 125525.

Bizzarro, M., Schiller, M., Yokoyama, T., Abe, Y., Aléon, J., Alexander, C. M. D., Amari, S., et al. 2023. The Magnesium Isotope Composition of Samples Returned from Asteroid Ryugu. *The Astrophysical Journal Letters* 958: L25.

Burkhardt, C., Kleine, T., Dauphas, N., and Wieler, R. 2012. Nucleosynthetic Tungsten Isotope Anomalies in Acid Leachates of the Murchison Chondrite: Implications for Hafnium–Tungsten Chronometry. *The Astrophysical Journal Letters* 753: L6.

Burkhardt, C., Kleine, T., Oberli, F., Pack, A., Bourdon, B., and Wieler, R. 2011. Molybdenum Isotope Anomalies in Meteorites: Constraints on Solar Nebula Evolution and Origin of the Earth. *Earth and Planetary Science Letters* 312: 390–400.

Dauphas, N., Marty, B., and Reisberg, L. 2002. Molybdenum Nucleosynthetic Dichotomy Revealed in Primitive Meteorites. *The Astrophysical Journal* 569: L139–L142.

Dauphas, N., and Schauble, E. A. 2016. Mass Fractionation Laws, Mass-Independent Effects, and Isotopic Anomalies. *Annual Review of Earth and Planetary Sciences* 44: 709–783.

Davidson, J., Busemann, H., Nittler, L. R., Alexander, C. M. D., Orthous-Daunay, F.-R., Franchi, I. A., and Hoppe, P. 2014. Abundances of Presolar Silicon Carbide Grains in Primitive Meteorites Determined by NanoSIMS. *Geochimica et Cosmochimica Acta* 139: 248–266.

Ek, M., Hunt, A. C., Lugaro, M., and Schönbächler, M. 2020. The Origin of *s*-Process Isotope Heterogeneity in the Solar Protoplanetary Disk. *Nature Astronomy* 4: 273–281.

Elfers, B.-M., Sprung, P., Messling, N., and Muenker, C. 2020. The Combined Zr and Hf Isotope Inventory of Bulk Rock and Sequentially Leached Chondrite Samples. *Geochimica et Cosmochimica Acta* 270: 475–491.

Fischer-Gödde, M., Burkhardt, C., Kruijer, T. S., and Kleine, T. 2015. Ru Isotope Heterogeneity in the Solar Protoplanetary Disk. *Geochimica et Cosmochimica Acta* 168: 151–171.

Hopp, T., Dauphas, N., Abe, Y., Aléon, J., Alexander, C. M. O'D., Amari, S., Amelin, Y., et al. 2022. Ryugu's Nucleosynthetic Heritage from the Outskirts of the Solar System. *Science Advances* 8: eadd8141.

Hu, Y., Moynier, F., Dai, W., Paquet, M., Yokoyama, T., Abe, Y., Aléon, J., et al. 2024. Pervasive Aqueous Alteration in the Early Solar System Revealed by Potassium Isotopic Variations in Ryugu Samples and Carbonaceous Chondrites. *Icarus* 409: 115884.

Huss, G. R., and Lewis, R. S. 1995. Presolar Diamond, SiC, and Graphite in Primitive Chondrites: Abundances as a Function of Meteorite Class and Petrologic Type. *Geochimica et Cosmochimica Acta* 59: 115–160.

Iizuka, T., Lai, Y.-J., Akram, W., Amelin, Y., and Schönbächler, M. 2016. The Initial Abundance and Distribution of ^{92}Nb in the Solar System. *Earth and Planetary Science Letters* 439: 172–181.

Jansen, C. A., Burkhardt, C., Marrocchi, Y., Schneider, J. M., Wölfer, E., and Kleine, T. 2024. Condensate Evolution in the Solar Nebula Inferred from Combined Cr, Ti, and O Isotope Analyses of Amoeboid Olivine Aggregates. *Earth and Planetary Science Letters* 627: 118567.

Kashiv, Y., Cai, Z., Lai, B., Sutton, S. R., Lewis, R. S., Davis, A. M., Clayton, R. N., et al. 2001. Synchrotron X-Ray Fluorescence: A New Approach for Determining Trace Element Concentrations in Individual Presolar SiC Grains. *32nd Lunar and Planetary Science Conference*, abstract #2192.

Kashiv, Y., Davis, A., Gallino, R., Cai, Z., Lai, B., Sutton, S., and Clayton, R. 2010. Extinct ^{93}Zr in Single Presolar SiC Grains from Low Mass Asymptotic Giant Branch Stars and Condensation from Zr-Depleted Gas. *The Astrophysical Journal* 713: 212–19.

Liu, N., Stephan, T., Cristallo, S., Gallino, R., Boehnke, P., Nittler, L. R., Alexander, C. M. O'D., et al. 2019. Presolar Silicon Carbide Grains of Types Y and Z: Their Molybdenum Isotopic Compositions and Stellar Origins. *The Astrophysical Journal* 881: 28.

Lodders, K. 2021. Relative Atomic Solar System Abundances, Mass Fractions, and Atomic Masses of the Elements and their Isotopes, Composition of the Solar Photosphere, and Compositions of the Major Chondritic Meteorite Groups. *Space Science Reviews* 217: 1–33.

Marrocchi, Y., Piralla, M., and Tissot, F. L. 2023. Iron Isotope Constraints on the Structure of the Early Solar System. *The Astrophysical Journal Letters* 954: L27.

Minster, J., and Ricard, L. P. 1981. The Isotopic Composition of Zirconium. *International Journal of Mass Spectrometry and Ion Physics* 37: 259–272.

Moynier, F., Dai, W., Yokoyama, T., Hu, Y., Paquet, M., Abe, Y., Aléon, J., et al. 2022. The Solar System Calcium Isotopic Composition Inferred from Ryugu Samples. *Geochemical Perspectives Letters* 24: 1–6.

Nakamura, E., Kobayashi, K., Tanaka, R., Kunihiro, T., Kitagawa, H., Potiszil, C., Ota, T., et al. 2022. On the Origin and Evolution of the Asteroid Ryugu: A Comprehensive Geochemical Perspective. *Proceedings of the Japan Academy, Series B* 98: 227–282.

Nakanishi, N., Yokoyama, T., Ishikawa, A., Walker, R. J., Abe, Y., Aléon, J., Alexander, C. M. O. D., et al. 2023. Nucleosynthetic *s*-Process Depletion in Mo from Ryugu Samples Returned by Hayabusa2. *Geochemical Perspectives Letters* 28: 31–36.

Nakashima, D., Nakamura, T., Zhang, M., Kita, N. T., Mikouchi, T., Yoshida, H., Enokido, Y., et al. 2023. Chondrule-like Objects and Ca-Al-Rich Inclusions in Ryugu May Potentially be the Oldest Solar System Materials. *Nature Communications* 14: 532.

Nanne, J. A., Nimmo, F., Cuzzi, J. N., and Kleine, T. 2019. Origin of the Non-Carbonaceous–Carbonaceous Meteorite Dichotomy. *Earth and Planetary Science Letters* 511: 44–54.

Nguyen, A. N., Mane, P., Keller, L. P., Piani, L., Abe, Y., Aléon, J., Alexander, C. M. O'D., et al. 2023. Abundant Presolar Grains and Primordial Organics Preserved in Carbon-Rich Exogenous Clasts in Asteroid Ryugu. *Science Advances* 9: eadh1003.

Nicolussi, G. K., Davis, A. M., Pellin, M. J., Lewis, R. S., Clayton, R. N., and Amari, S. 1997. s-Process Zirconium in Presolar Silicon Carbide Grains. *Science* 277: 1281–83.

Paquet, M., Moynier, F., Yokoyama, T., Dai, W., Hu, Y., Abe, Y., Aléon, J., et al. 2023. Contribution of Ryugu-Like Material to Earth's Volatile Inventory by Cu and Zn Isotopic Analysis. *Nature Astronomy* 7: 182–89.

Pellin, M. J., Savina, M. R., Calaway, W. F., Tripa, C. E., Barzyk, J. G., Davis, A. M., Gyngard, F., et al. 2006. Heavy Metal Isotopic Anomalies in Supernovae Presolar Grains. *37th Lunar and Planetary Science Conference*, abstract #2041.

Render, J., and Brennecka, G. A. 2021. Isotopic Signatures as Tools to Reconstruct the Primordial Architecture of the Solar System. *Earth and Planetary Science Letters* 555: 116705.

Render, J., Brennecka, G. A., Burkhardt, C., and Kleine, T. 2022. Solar System Evolution and Terrestrial Planet Accretion Determined by Zr Isotopic Signatures of Meteorites. *Earth and Planetary Science Letters* 595: 117748.

Rüfenacht, M., Morino, P., Lai, Y.-J., Fehr, M. A., Haba, M. K., and Schönbächler, M. 2023. Genetic Relationships of Solar System Bodies Based on their Nucleosynthetic Ti Isotope Compositions and Sub-Structures of the Solar Protoplanetary Disk. *Geochimica et Cosmochimica Acta* 355: 110–125.

Sanders, I. S., and Scott, E. R. 2022. Complementary Nucleosynthetic Isotope Anomalies of Mo and W in Chondrules and Matrix in the Allende Carbonaceous Chondrite: The Case for Hydrothermal Metamorphism and Its Implications. *Meteoritics & Planetary Science* 57: 450–471.

Schiller, M., Van Kooten, E., Holst, J. C., Olsen, M. B., and Bizzarro, M. 2014. Precise Measurement of Chromium Isotopes by MC-ICPMS. *Journal of Analytical Atomic Spectrometry* 29: 1406–16.

Schönbächler, M., Lee, D. C., Rehkämper, M., Halliday, A. N., Fehr, M. A., Hattendorf, B., and Günther, D. 2003. Zirconium Isotope Evidence for Incomplete Admixing of *r*-Process Components in the Solar Nebula. *Earth and Planetary Science Letters* 216: 467–481.

Schönbächler, M., Rehkämper, M., Fehr, M. A., Halliday, A. N., Hattendorf, B., and Günther, D. 2005. Nucleosynthetic Zirconium Isotope Anomalies in Acid Leachates of Carbonaceous Chondrites. *Geochimica et Cosmochimica Acta* 69: 5113–22.

Schönbächler, M., Rehkämper, M., Lee, D.-C., and Halliday, A. N. 2004. Ion Exchange Chromatography and High Precision Isotopic Measurements of Zirconium by MC-ICP-MS. *Analyst* 129: 32–37.

Schrader, D. L., Cloutis, E. A., Applin, D. M., Davidson, J., Torrano, Z. A., Foustoukos, D., Alexander, C. M. D., et al. 2024. Tarda and Tagish Lake: Samples from the Same Outer Solar System Asteroid and Implications for D-and P-Type Asteroids. *Geochimica et Cosmochimica Acta* 380: 48–70.

Stephan, T., Trappitsch, R., Hoppe, P., Davis, A. M., Bose, M., Boujibar, A., Gyngard, F., et al. 2024. The Presolar Grain Database. I. Silicon Carbide. *The Astrophysical Journal Supplement Series* 270: 27.

Stephan, T., Trappitsch, R., Hoppe, P., Davis, A. M., Pellin, M. J., and Pardo, O. S. 2019. Molybdenum Isotopes in Presolar Silicon Carbide Grains: Details of *s*-Process Nucleosynthesis in Parent Stars and Implications for *r*- and P-Processes. *The Astrophysical Journal* 877: 101.

Sugita, S., Honda, R., Morota, T., Kameda, S., Sawada, H., Tatsumi, E., Yamada, M., et al. 2019. The Geomorphology, Color, and Thermal Properties of Ryugu: Implications for Parent-Body Processes. *Science* 364: eaaw0422.

Tachibana, S., Sawada, H., Okazaki, R., Takano, Y., Sakamoto, K., Miura, Y., Okamoto, C., et al. 2022. Pebbles and Sand on Asteroid (162173) Ryugu: In Situ Observation and Particles Returned to Earth. *Science* 375: 1011–16.

Tissot, F. L. H., Ibañez-Mejia, M., Rabb, S. A., Kraft, R. A., Vocke, R. D., Fehr, M. A., Schönbächler, M., Tang, H., and Young, E. D. 2023. A Community-Led Calibration of the Zr Isotope Reference Materials: NIST Candidate RM 8299 and SRM 3169. *Journal of Analytical Atomic Spectrometry* 38: 2087–2104.

Torrano, Z. A., Alexander, C. M. D., Carlson, R. W., Render, J., Brennecka, G. A., and Bullock, E. S. 2024. A Common Isotopic Reservoir for Amoeboid Olivine Aggregates (AOAs) and Calcium-Aluminum-Rich Inclusions (Cais) Revealed by Ti and Cr Isotopic Compositions. *Earth and Planetary Science Letters* 627: 118551.

Torrano, Z. A., Jordan, M. K., Mock, T. D., Carlson, R. W., Gautam, I., Haba, M. K., Yokoyama, T., et al. 2023. Neodymium-142 Deficits and Samarium Neutron Stratigraphy of C-Type Asteroid (162173) Ryugu. *Meteoritics & Planetary Science* 59: 1966–82.

Travaglio, C., Gallino, R., Arnone, E., Cowan, J., Jordan, F., and Sneden, C. 2004. Galactic Evolution of Sr, Y, and Zr: A Multiplicity of Nucleosynthetic Processes. *The Astrophysical Journal* 601: 864–884.

Trinquier, A., Elliott, T., Ulfbeck, D., Coath, C., Krot, A. N., and Bizzarro, M. 2009. Origin of Nucleosynthetic Isotope Heterogeneity in the Solar Protoplanetary Disk. *Science* 324: 374–76.

Yap, T. E., and Tissot, F. L. 2023. The NC-CC Dichotomy Explained by Significant Addition of Cai-Like Dust to the Bulk Molecular Cloud (BMC) Composition. *Icarus* 405: 115680.

Yokoyama, T., Alexander, C. M. D., and Walker, R. J. 2011. Assessment of Nebular Versus Parent Body Processes on Presolar Components Present in Chondrites: Evidence from Osmium Isotopes. *Earth and Planetary Science Letters* 305: 115–123.

Yokoyama, T., Nagai, Y., Fukai, R., and Hirata, T. 2019. Origin and Evolution of Distinct Molybdenum Isotopic Variabilities within Carbonaceous and Noncarbonaceous Reservoirs. *The Astrophysical Journal* 883: 62.

Yokoyama, T., Nagashima, K., Nakai, I., Young, E. D., Abe, Y., Aléon, J., Alexander, C. M. O. D., et al. 2023a. Samples Returned from the Asteroid Ryugu Are Similar to Ivuna-Type Carbonaceous Meteorites. *Science* 379: eabn7850.

Yokoyama, T., Nagashima, K., Nakai, I., Young, E. D., Abe, Y., Aléon, J., Alexander, C. M. O'D., et al. 2023b. Water Circulation in Ryugu Asteroid Affected the Distribution of Nucleosynthetic Isotope Anomalies in Returned Sample. *Science Advances* 9: eadi7048.

Zinner, E. 2014. Presolar Grains. In *Treatise on Geochemistry*, edited by A. M. Davis, vol. 2, 181–213. Amsterdam: Elsevier.

SUPPORTING INFORMATION

Additional supporting information may be found in the online version of this article.

Data S1. Verification of the accuracy of the Zr isotope data.

Table S1. Zr isotope data for sample purity and doping tests.

Table S2. Zr isotope data for terrestrial samples.

Table S3. Zr isotope data for Ryugu and meteorites.